The reticulocyte restriction: invasion ligand RBP1a of *Plasmodium vivax* targets human TfR1, prohibitin-2, and basigin

Jessica Molina-Franky[1-4], Daniel Röth[1], Monica Ararat-Sarria[3,5], Manuel Alfonso Patarroyo[3,6*], Markus Kalkum[1*]

[1]Department of Immunology and Theranostics, Arthur Riggs Diabetes and Metabolism Research Institute, Beckman Research Institute of the City of Hope, Duarte, California, United States of America

[2]Global Scholars Program, Beckman Research Institute of the City of Hope, Duarte, California, United States of America

[3]Grupo de Investigación Básica en Biología Molecular e Inmunología (GIBBMI), Fundación Instituto de Inmunología de Colombia (FIDIC), Bogotá, Colombia

[4]PhD Program in Biotechnology, Universidad Nacional de Colombia, Bogotá, Colombia

[5]Health Sciences Faculty, Universidad de Ciencias Aplicadas y Ambientales (U.D.C.A), Bogotá, Colombia

[6]Microbiology Department, Faculty of Medicine, Universidad Nacional de Colombia, Bogotá, Colombia

[*] Corresponding authors:

E-mail: mkalkum@coh.org (MK)

E-mail: mapatarr.fidic@gmail.com (MAP)

Abstract

Plasmodium vivax is the most widespread malaria species with predominance in Latin America and Southeast Asia. Devising effective controls against *P. vivax* infections presents unique challenges due to the parasite's exclusive invasion of reticulocytes, a transient developmental stage of red blood cells. The ephemeral nature and limited availability of reticulocytes complicate efforts to establish continuous *in vitro* cultures to study the parasite's biology and receptor-ligand interactions. Here, the potential of the erythroid cell lines JK-1 and BEL-A as alternatives to reticulocytes was confirmed through successful parasite invasion, marking the first report of *P. vivax* entry to BEL-A cells. Furthermore, LC-MS was used to quantitatively compare the membrane proteomes of these cell lines with those of reticulocytes and mature erythrocytes. This analysis revealed significant similarities between the membrane proteomes of JK-1, BEL-A, and reticulocytes. In addition to the known *Plasmodium* receptors, transferrin receptor protein 1 (TfR1 or CD71), CD98hc, and basigin (BSG), potential receptor candidates involved in the parasite's invasion pathway were identified, including prohibitin-2 (PHB2), CAT-1 (SLC7A1), ATB(0) (SLC1A5), CD36, integrin beta-1 (ITGB1), and Metal transporter CNNM3. Proximity labeling using TurboID enabled the identification of specific interactions between PvRBP1a$_{158-650}$ and TfR1, BSG, and prohibitin-2 in the erythroid cell lines. Notably, this is the first report of prohibitin-2 as a receptor for *P. vivax*. These findings advance the understanding of *P. vivax* receptor-ligand interactions and underscore the potential of JK-1 and BEL-A cell lines as alternative models for the study of parasite biology.

Author Summary

Plasmodium vivax is a major cause of malaria, particularly in Latin America and Southeast Asia. Unlike other malaria parasites, it infects only immature red blood cells (reticulocytes), which are rare and short-lived, making laboratory studies challenging. No continuous *in vitro* culture system currently exists for *P. vivax*, limiting research into its invasion mechanisms. In this study, we evaluated two erythroid cell lines, JK-1 and BEL-A, as potential reticulocyte surrogates. We demonstrate that *P. vivax* can invade both cell types, including BEL-A cells, which had not previously been tested. Comparative analysis revealed key differences in surface protein expression between these cell lines and reticulocytes, compared to mature red blood cells, identifying seven potential parasite-receptor proteins. We further applied a proximity-based protein tagging approach to identify host-parasite interactions mediated by a specific *P. vivax* protein ligand, RBP1a. This technique revealed a potential role for prohibitin-2, TfR1, and basigin in mediating *P. vivax* entry into red blood cells by RBP1a binding. The role of prohibitin-2 as a Plasmodium receptor is a novel Discovery. Our results highlight JK-1 and BEL-A cells as valuable tools for *P. vivax* research and suggest new avenues for investigating host-pathogen interactions, with implications for malaria treatment and vaccine development.

Introduction

Malaria remains a major global health issue, with 263 million cases reported in 2023. *Plasmodium vivax*, one of the six human-infecting *Plasmodium* species, is noteworthy for its global distribution. In the Americas, most malaria cases are due to *P. vivax* (72.1% in 2023) [1]. Its blood stage form, the merozoites, interact with red blood cell

73 (RBC) receptors leading to RBC invasion [2–4]. However, *P. vivax* exclusively infects
74 reticulocytes [5], immature, short-lived precursors of erythrocytes, posing a significant
75 challenge to research progress. In contrast, *P. falciparum* has been extensively
76 researched due to the availability of a well-established *in vitro* culture system for over 40
77 years [6]. This critical disparity highlights the urgent need to develop alternative
78 research models for *P. vivax*.
79 The mechanism of *P. vivax* reticulocyte invasion remains unclear. It was previously
80 believed that *P. vivax* exclusively targeted reticulocytes through the Duffy antigen
81 receptor for chemokines (DARC) and Duffy binding protein (PvDBP) interaction [7], as
82 individuals with the Fy(a-b-) mutation in West Africa were resistant to the infection.
83 However, DARC is present on both reticulocytes and erythrocytes, and *P. vivax*
84 infections have been documented in Duffy-negative populations [8–10]. Current
85 evidence suggests that the reticulocyte-binding protein (RBP) family may play a role,
86 interacting with transferrin receptor 1 (TfR1) and CD98 heavy chain (SLC3A2), which
87 are lost during the maturation of reticulocytes to erythrocytes [2,3,11]. This implies that
88 *P. vivax (*Pv*)*RBP family proteins may specifically target receptors unique to the
89 reticulocyte membrane. Our previous studies on PvRBP1 of the *P. vivax* strain Belem
90 (GenBank AAA29743.3) identified eleven high-affinity reticulocyte binding peptides
91 (HABPs) corresponding to residues 158–653 of PvRBP1a in the *P. vivax* Salvador I
92 strain (GenBank AAS85749.1). Among these, HABP 3742 (KLLGEEISEVSHLYV) and
93 HABP 3459 (KEILDKMAKKVHYLK) exhibited dissociation constants (*K*d) of 131 nM
94 and 155 nM, respectively [12]. Additionally, an extracellular portion of PvRBP1a,
95 residues 157-650, binds strongly (~50%) to reticulocytes and moderately (~20%) to

96 erythrocytes [13]. The identity of PvRBP1a$_{157-650}$ binding-receptors within the
97 reticulocyte membrane has been unclear. Therefore, this study evaluated the
98 erythroleukemic cell line JK-1 [14] and the Bristol Erythroid Line Adult (BEL-A) [15] as
99 surrogates for reticulocytes, examining their susceptibility to *P. vivax* invasion. A
100 comparison of the cell lines' membrane proteomes revealed similarities with those of
101 reticulocytes, and dissimilarities with erythrocyte membrane proteomes, thereby
102 identifying potential *P. vivax* receptors. Furthermore, TurboID proximity labelling implied
103 specific interactions of PvRBP1a$_{158-650}$ with prohibitin-2 (PHB2), TfR1, and basigin
104 (BSG). These interactions were confirmed by ELISA, highlighting key molecular
105 determinants of *P. vivax*'s reticulocyte tropism.

106 Results

107 *P. vivax* can invade the erythroid cell lines BEL-A and JK-1

108 Cultured BEL-A and JK-1 cells were successfully invaded by *P. vivax* from a validated
109 mono-infected malaria patient's blood sample. The experiment required forgoing
110 enrichment of the RBCs to 4.0% parasitemia (Fig 1 A-E). Parasite invasion was
111 confirmed by immunofluorescence microscopy, detecting the intracellular presence of *P.*
112 *vivax* lactate dehydrogenase (PvLDH), which all blood stages of the parasite are known
113 to express [16]. PvLDH was detected in the positive control of infected reticulocytes,
114 and in BEL-A and JK-1 cells, incubated with infected reticulocytes (Fig 2, FITC). The
115 PvLDH signal was absent from non-infected control cells. Moreover, the presence of
116 hemozoin (Hz) pigment, characteristic for hemoglobin consumption by *Plasmodia* within
117 infected RBCs [17], was observed (Fig 2, bright field, and merge). The dark Hz pigment
118 was visible inside the parasite-infected nucleated erythroid cells as well as in infected

119 reticulocytes that originated from the donor. Hz is an insoluble, crystallized digestion
120 product of heme derived from the digestion of hemoglobin by malaria parasites,
121 containing heme-derived β-hematin, which neutralizes the toxicity of free heme released
122 after parasite invasion through a digestive process that involves the digestive vacuole
123 structure [18]. On days 3 to 6 post-infection, no parasite-infected erythroid cells were
124 observed, and cell mortality had substantially increased. Therefore, the experiment was
125 stopped on day 6.

126 **Fig 1**. ***P. vivax* mono-infected reticulocytes.** (A) Three representative micrographs of
127 *P. vivax*-infected enriched reticulocytes (red arrows) from a malaria patient. Scale bars
128 are 3 μm. (B-D) Species-specific nested PCR for the small subunit 18S ribosomal RNA.
129 Lane M, 100 bp marker; Lane *PvSx*, sample used in the infection of erythroid cells;
130 Lanes *Pv*, *Pf*, and *Pm* belong to the positive controls for each species; lane NCh,
131 negative control using genomic DNA from a healthy human; lane NC, negative control
132 using water instead of genomic DNA. (B) *P. vivax* (~120 bp amplicon). (C) *P. falciparum*
133 (~205 bp amplicon). (D) *P. malariae* (~144 bp amplicon). (E) DNA sequence alignment
134 of the positive *PvSx* amplicon with the corresponding gene segment of the *P. vivax*
135 Salvador-1 reference strain (GenBank No. XR_003001206.1) [19], showing 100%
136 identity.

137 **Fig 2. *P. vivax* invades BEL-A and JK-1 cells.** The micrographs show *P. vivax*-
138 infected reticulocytes as the positive Control (+); infected BEL-A and JK-1 cells at 24
139 and 48 h, and their non-infected negative Control (-); *P. vivax* lactate dehydrogenase
140 (FITC green); DNA (DAPI blue); hemozoin crystals (black dots marked with red arrows);
141 BF (bright field); Scale bars are 5 μm.

142 ## Overlapping membrane proteomes reveal potential *P. vivax*
143 ## invasion receptors

144 Because *P. vivax* was able to invade the erythroid BEL-A and JK-1 cells, their
145 membranes must contain the same essential receptor molecules as reticulocytes that
146 enable parasite invasion. Furthermore, the membranes of mature erythrocytes are
147 expected to lack these receptors or to express them only at insufficient abundances.
148 Consequently, a quantitative comparison of the membrane proteome of these cells with
149 those of human reticulocytes and erythrocytes identified potential receptors for *P. vivax*
150 merozoite ligands that are most likely responsible for its reticulocyte-restricted invasion.
151 Stringent isolation procedures were necessary to obtain membrane proteins of pure
152 reticulocytes. The isolated reticulocytes ($CD71^+$, $CD45^-$) used in this proteomic
153 comparison had a purity of 98.4% (S2 Fig). Expression of CD71 is diminished during
154 maturation into fully functional erythrocytes [20]. Simultaneous determination of CD45
155 negativity was necessary, as $CD45^+$ leukocytes also express CD71, to ensure purity of
156 the isolated reticulocytes.
157 The BEL-A and JK-1 cells used in the membrane proteomic comparisons were
158 harvested from *in vitro* cultures and exhibited distinct nucleated erythroid maturation
159 stages, including proerythroblasts, basophilic erythroblasts, polychromatic erythroblasts,
160 and orthochromatic erythroblasts (S3 Fig), with slight dominance of the basophilic and
161 polychromatic stages.
162 In total, 2,100 proteins were identified in BEL-A cells and 2,178 in JK-1 cells. The
163 number of proteins was lower in reticulocytes (1,234) and in erythrocytes (1,347). After
164 filtering this data for membrane proteins (see S1 Text & S4 Fig), 1,530 and 1,595 such

165 proteins were obtained from BEL-A and JK-1 cell ghosts, respectively, while 846 and
166 974 proteins were identified for reticulocyte and erythrocyte ghosts.
167 Changes in membrane protein abundance were assessed by comparing erythroid cell
168 lines and reticulocytes to mature erythrocytes. The protein abundancies of reticulocytes
169 clustered better with those of BEL-A and JK-1 cells than with those of erythrocytes (Fig
170 3A). It was found that compared to erythrocytes 256 proteins were more abundant in
171 reticulocytes, 1,179 in JK-1, and 1,554 in BEL-A. Of these, 144 identical proteins were
172 increased in reticulocytes, JK-1, and BEL-A. However, reticulocytes and JK-1 cells
173 share 18 proteins that are less abundant in erythrocytes, while BEL-A and reticulocytes
174 have 40 proteins in common, that are less abundant in erythrocytes. Only 54 membrane
175 proteins with higher abundance than in erythrocytes were identified exclusively in
176 reticulocytes, 237 in JK-1, and 590 in BEL-A cells (Fig 3B).
177 **Fig 3. Plasma membrane proteomes of reticulocytes resemble those of erythroid**
178 **cell lines.** (A) Clustering of plasma membrane proteins in JK-1, BEL-A, reticulocytes,
179 and erythrocytes, measured in triplicate. Log2 intensities. (B) Abundance of intersecting
180 membrane proteins in reticulocytes, JK-1, and BEL-A cells compared to erythrocytes,
181 represented in an UpSet plot [21]. 144 proteins share higher abundance among cell
182 lines and reticulocytes but are reduced in erythrocytes (mauve bar). (C-E) Putative
183 receptors (blue) and characterized receptors (orange) for *P. vivax* merozoite invasion.
184 Gene names are displayed instead of protein names for simplicity. The x-axis
185 represents the $\log_2$ fold change, and the y-axis shows the P-value, indicating statistical
186 significance.

187 When comparing the membrane protein abundance in reticulocytes, cell lines, and
188 erythrocytes, known *P. vivax* receptors such as TfR1 (CD71), CD98hc, ACKR1/DARC,
189 BSG, CR1, and band 3 (SLC4A1) were identified. TfR1 and CD98hc, which are lost
190 during reticulocyte maturation to erythrocytes, were significantly more abundant in
191 reticulocytes and cell lines. In contrast, the other receptors showed higher levels in
192 erythrocytes (Fig 3C-E).
193 *In silico* topological analysis of membrane proteins enriched in reticulocytes and
194 erythroid cell lines identified several candidates — CD98lc (SLC7A5), high-affinity
195 cationic amino acid transporter 1 (CAT-1, SLC7A1), neutral amino acid transporter B^0
196 (ATB(0), SLC1A5), CD36, Integrin β-1 (ITGB1), prohibitin-2 (PHB2), and the metal
197 transporter CNNM3 — as possessing sizable extracellular regions that are potentially
198 accessible for interaction with *P. vivax* merozoite ligands (S1 Table & S5 Fig).
199 The significantly higher abundance of these proteins in reticulocytes, BEL-A, and JK-1
200 cells compared to erythrocytes (Fig 3C-E & S1 Table) highlights them as potential
201 candidates for *P. vivax* merozoite protein receptors, which may explain the parasite's
202 exclusivity for reticulocyte invasion.

203 Receptors for PvRBP1a$_{158-650}$LTID identified via proximity
204 labeling

205 To identify potential receptors of the PvRBP1a$_{158-650}$LTID protein, the TurboID proximity
206 labeling technique was used. This technique enables the biotinylation of proteins that
207 come into close contact with the fused protein (within 10 nm), facilitating the
208 identification of their interactions [22,23]. Therefore, the fusion protein PvRBP1a$_{158-}$
209 $_{650}$LTID and the LTID control were obtained in soluble form, with PvRBP1a$_{158-650}$LTID

210 having a molecular weight of ~94 kDa and LTID ~36 kDa (Fig 4A). Both proteins
211 exhibited enzymatic activity and self-biotinylation at 1, 2, and 3 μM (Fig 4B-C).

212 **Fig 4. Proximity labeling with PvRBP1a$_{158-650}$LTID in JK-1, BEL-A, reticulocytes,**
213 **and erythrocytes.** Recombinantly expressed soluble PvRBP1a$_{158-650}$LTID and LTID by
214 (A) SDS PAGE (B, C) auto-biotinylation assay with increasing concentrations of each
215 protein at 1, 2, and 3 μM, detected with IRDye 800 Streptavidin (green bands),
216 LICORbio molecular weight markers (MW, red bands); (D) biotin labeling of JK-1
217 (orange) and BEL-A (fuchsia) cells, in presence of PvRBP1a$_{158-650}$LTID or LTID
218 (negative control, JK-1 - black, and BEL-A - gray) at 1, 2, and 3 μM. (E-G) Flow
219 cytometry (E) histograms of erythroid cells and human RBCs in presence of
220 PvRBP1a$_{158-650}$LTID (blue) or LTID (grey), both at 3 μM, demonstrating (F) significant
221 degrees of cell surface labeling by PvRBP1a$_{158-650}$LTID in erythroid cells and
222 reticulocytes compared to erythrocytes (**** $p \leq 0.0001$). (G) Receptors to PvRBP1a$_{158-}$
223 $_{650}$ are sensitive to cell surface treatment with trypsin and chymotrypsin but resistant to
224 neuraminidase (labeling % as normalized to untreated cells).

225 PvRBP1a$_{158-650}$LTID exhibits comparable binding to reticulocytes and
226 erythroid cell lines via a proteinaceous receptor

227 Proximity biotinylation mediated by TurboID facilitated binding evaluation through the
228 biotin-streptavidin interaction. The assays showed that PvRBP1a$_{158-650}$LTID binding is
229 concentration-dependent (Fig 4D). Since the highest percentage of biotin labeling on
230 the cell surface was obtained at 3 μM, this concentration was selected to analyze
231 PvRBP1a$_{158-650}$LTID binding to enriched reticulocytes (87.5% purity) (S6 Fig),
232 erythrocytes, and cell lines. The results showed that PvRBP1a$_{158-650}$ had 80%

233 biotinylation on the surface of reticulocytes, 4.7% on erythrocytes, and 79.85% and
234 83.2% on the surface of JK-1 and BEL-A cells, respectively. A statistically significant
235 difference was found between the cell lines and reticulocytes compared to erythrocytes
236 ($P \leq 0.0001$). However, no significant difference was observed between the cell lines
237 and reticulocytes (Fig 4E-F). These data suggest that erythroid cell lines exhibit
238 PvRBP1a$_{158\text{-}650}$ binding activity comparable to reticulocytes, indicating that they may
239 express the receptor for this specific *P. vivax* ligand on their surface. Additionally, no
240 labelling was detected with LTID, confirming the specificity of the PvRBP1a$_{158\text{-}650}$
241 receptor interaction.
242 Cell surface labelling with PvRBP1a$_{158\text{-}650}$LTID was sensitive to trypsin and
243 chymotrypsin treatment but resistant to neuraminidase, which removes sialic acid from
244 glycans that modify proteins in vertebrates (Fig 4G). Therefore, the cell surface receptor
245 function for PvRBP1a$_{158\text{-}650}$ is proteinaceous and not dependent on sialic acid-
246 terminated glycans.

247 Enrichment of PvRBP1a$_{158\text{-}650}$LTID biotinylated cell surface proteins, 248 identifies TfR1 and prohibitin-2 as the likely reticulocyte-restricting 249 receptors

250 PvRBP1a$_{158\text{-}650}$LTID biotinylated membrane proteins from erythroid cells were captured
251 via streptavidin-affinity and subjected to proteomics analysis, revealing a total of 278
252 proteins, of which 12 were localized to the plasma membrane. However, the LTID
253 control contained five of these proteins, leaving seven unique to enrichment after
254 biotinylation with PvRBP1a$_{158\text{-}650}$LTID. Four of these membrane proteins do not possess
255 extracellular regions, while TfR1, prohibitin-2, and BSG do. Such extracellular regions

256 should be required to facilitate an interaction with *P. vivax* merozoite ligands (Fig 5A).
257 Interaction of PvRBP1a$_{158-650}$ was successfully validated by targeted (PRM) LC-MS
258 analysis for TfR1, BSG, and prohibitin-2 (Fig 5B). It clearly demonstrated that only
259 PvRBP1a$_{158-650}$LTID biotinylated these three proteins, while LTID did not.
260 BSG is more abundant in erythrocytes than in reticulocytes and in the erythroid cell
261 lines. In contrast, TfR1 and prohibitin-2 were significantly less abundant in erythrocytes
262 (Fig 3C-E). In fact, TfR1 and prohibitin-2 were among the most abundant membrane
263 proteins in reticulocytes and in the erythroid cell lines JK-1 and BEL-A. These findings
264 suggest that PvRBP1a$_{158-650}$ likely facilitate the recognition and invasion of reticulocytes
265 through interaction with TfR1 and prohibitin-2.
266 **Fig 5. Proximity biotin-labeled TfR1 (CD71), Basigin, and Prohibitin-2, are**
267 **identified as *P. vivax* receptor candidates after interaction of JK-1 cells with**
268 **PvRBP1a$_{158-650}$LTID and validated by targeted LC-MS.** (A) Heatmap of labeled
269 plasma membrane protein intensities in the PvRBP1a$_{158-650}$LITD (fuchsia) and LTID
270 (yellow) control samples, analyzed in duplicate by DDA LC-MS proteomics. Intensities
271 are represented on a Z-score scale, where each value was transformed by the number
272 of standard deviations (SD) from the mean. Topology categorizes proteins by their
273 cellular localization: intracellular (Inside, dark gray) and those with extracellular domains
274 (Outside, cyan). They include Shroom3, GPR132 – probable G-protein coupled receptor
275 132, EEF1A1 – Elongation factor 1-alpha 1, protein S100-A8, protein S100-A6, TfR1,
276 PHB2 – prohibitin-2, BSG, protein S100-A9, JUP – junction plakoglobin, DSC3 –
277 Desmocollin-3, and VIM – vimentin. (B) Validated interactions of transferrin receptor 1,
278 basigin, and prohibitin-2 with PvRBP1a$_{158-650}$LITD, but not with LITD, during the TurboID

279 procedure, followed by PRM LC-MS. (1) (2) – duplicates. Stacked bars are the sum of
280 the LC-MS ion chromatographic peak areas of the trypsin digested peptides (colored
281 boxes) of each protein, indicating the contribution of each peptide to the individual
282 protein abundance.

283 PvRBP1a$_{158-650}$LTID interacts with high-affinity binding to
284 TfR1, BSG, and prohibitin-2

285 The titration curves fit well to a single-site binding saturation model. In contrast, the
286 negative control LTID displayed a nonspecific binding pattern "unstable", corroborating
287 the specificity of the interactions (Fig 6A). The Kd obtained from the ELISA titration
288 indicated that PvRBP1a$_{158-650}$LTID had high affinity for TfR1 (Kd: 1.15 nM), followed by
289 BSG (Kd: 2.16 nM) and prohibitin-2 (Kd: 2.77 nM) (Fig 6B).

290 **Fig 6. PvRBP1a$_{158-650}$ binds to TfR1, BSG, and PHB2 at nanomolar affinities.** (A)
291 Titration ELISAs of protein-protein interactions between soluble ligand PvRBP1a$_{158-}$
292 $_{650}$LTID, control LTID, and the immobilized receptor candidates TfR1, BSG, and PHB2.
293 OD_{450} absorbance values represent the binding of a TurboID-specific HRP-labeled
294 antibody for the biotin-free quantification of ligand and control in triplicate, fitted by a
295 single-site binding model; (B) average dissociation constants (kd) summarized as
296 determined from the fitted titration curves above.

297 Discussion

298 This study demonstrates the utility of erythroid cell lines JK-1 and BEL-A as suitable
299 surrogates for reticulocytes for studying the invasion process of the *P. vivax* malaria
300 parasite. While these cell lines and their culture conditions did not support a continuous

301 *P. vivax* culture *in vitro*, the formation of the Hz pigment and immuno detection of
302 PvLDH strongly supported parasite invasion. In contrast to human reticulocytes, both
303 erythroid cell lines are nucleated, which might permit them to initiate a cell-death
304 program upon parasite invasion. Consistently, JK-1 cells were previously reported to
305 support cell entry by both *P. vivax* and *P. falciparum* [24,25], while BEL-A cells have so
306 far only been studied with *P. falciparum* [26]. This study is the first to report *P. vivax*
307 invasion of BEL-A cells, confirming their susceptibility alongside JK-1 cells.
308 The quantitative membrane proteome comparison of reticulocytes and erythroid cell
309 lines with erythrocytes revealed Prohibitin-2 (PHB2), TfR1 (CD71), the CD98 heavy
310 chain (4F2hc, gene SLC3A2), the CD98 light chain (LAT-1, gene SLC7A5), ATB(0)
311 (gene SLC1A5), CAT-1 (SLC7A1), CD36, Integrin β-1 (gene ITGB1), and Metal
312 transporter CNNM3 to be of significantly increased abundance in those cell lines and
313 reticulocytes. Whereas they are strongly decreased (practically absent) in fully matured
314 erythrocytes. The increased abundance of TfR1 and CD98 in reticulocytes over
315 erythrocytes is consistent with previous studies [2,20]. However, genetic manipulation
316 [3] or antibody blockade [2] of these proteins only partially reduced *P. vivax* invasion,
317 suggesting the involvement of additional receptors. The heavy chain of CD98 (SLC3A2)
318 was reported to be bound by *P. vivax* in immature red blood cells via PvRBP2a [2].
319 Therefore, other potential *P. vivax* receptor candidates with extracellular regions,
320 namely Prohibitin-2, the CD98 light chain (LAT-1), ATB(0), CAT-1, CD36, Integrin β-1,
321 and CNNM3 should be considered. These membrane proteins participate in various
322 protein-protein interactions that facilitate the entry of microorganisms into host cells [27–
323 39]. Interestingly, LAT-1, that together with its heavy chain 4F2hc forms the heteromeric

324 CD98 [40,41], plays a role in hepatitis C virus entry [42], raising the question of whether
325 *P. vivax* may also interact with LAT-1.
326 Proximity labeling of erythroid cells with PvRBP1a$_{158-650}$LTID was largely consistent with
327 previous observations, in which ~50% of reticulocytes binding and ~20% of erythrocytes
328 bound to PvRBP1a$_{157-650}$ [13]. Furthermore, 20 of reticulocytes and only 1% of
329 erythrocytes bound to PvRBP1a$_{351-599}$ [43], while 31.5% of reticulocytes were reported to
330 bind to PvRBP1a$_{30-778}$ [44]. Additionally, the trypsin and chymotrypsin sensitivity of these
331 recombinant protein [13,43,44], as well as the PvRBP1a$_{157-653}$ HAPBs [12] align with our
332 results.
333 PvRBP1a$_{158-650}$ was found to interact with Prohibitin-2, TfR1, and BSG. Prohibitin-2 and
334 TfR1 are more abundant in reticulocyte membranes and cell lines compared to
335 erythrocytes, while BSG is more abundant in erythrocytes. These findings suggest that
336 PvRBP1a$_{158-650}$ may facilitate reticulocyte recognition and invasion through interaction
337 with Prohibitin-2 and TfR1. Additionally, interaction with BSG may contribute to binding
338 activity to erythrocytes, but not their restricted invasion, consistent with previous studies
339 on PvRBP1a binding [12,13,43,44].
340 This study demonstrated strong binding of PvRBP1a$_{158-650}$ with the 89-760 domain of
341 TfR1, contrasting with prior work that did not detect this interaction, possibly due to the
342 crucial role of TfR1's 89-120 region, not included in the previous protein construct [25].
343 TfR1 is a known receptor for PvRBP2b [3], as well as for various New World
344 arenaviruses [45,46]. BSG, a known receptor for *P. falciparum* RH5 [47,48], a member
345 of the PfRH family homologous to the PvRBP proteins of *P. vivax* [49,50], also serves
346 as a receptor for *P. vivax* TRAg38 [51]. Similarly, prohibitin-2, facilitates viral entry into

347 host cells, including enteroviruses, coronaviruses, HIV-1, and flaviviruses such as
348 dengue [39,52–54].
349 This research demonstrated the binding versatile of PvRBP1a$_{158-650}$, which interacts
350 with three different membrane proteins. In biological systems, ligands often bind
351 multiple receptors, as seen with *Plasmodium* interactions; PvTRAg38 binds both BSG
352 and band 3 [51,55], and PfEMP1binds to several receptors [56–60].
353 This study demonstrates that the BEL-A and JK-1 cells are suitable models for studying
354 *P. vivax* receptor-ligand interactions, providing viable alternatives to reticulocytes. The
355 similarity in the abundance of potential receptor candidates between cell lines and
356 reticulocytes, and their dissimilarity with erythrocytes, validates the use of JK-1 and
357 BEL-A cell lines as surrogate models for the study of *P. vivax* merozoite ligand-receptor
358 interactions, and suggests the existence of other potential *P. vivax* receptors. prohibitin-
359 2 and TfR1 may contribute to a redundant reticulocyte-restricted invasion pathway
360 because they exhibit high binding affinities to PvRBP1a$_{158-650}$. These findings lay the
361 foundation for the comprehensive study of all *P. vivax* invasion mechanisms and for the
362 development of targeted therapies against malaria.

363 Materials and methods

364 Ethics statement

365 The study was conducted in accordance with the Declaration of Helsinki. Use of
366 anonymized discarded blood from therapeutic phlebotomy was approved by the
367 Institutional Review Board of City of Hope, Duarte, California, USA, as exempt category
368 4, under 45CFR46.104 (d). Blood samples from malaria patients were obtained under
369 informed consent with the approval of the Bioethics central committee of the

370 Universidad de Córdoba, Monteria, Colombia, and imported into the United States
371 under CDC permit No.: 20210830-3188A0.

372 Collection, processing, and enrichment of *P. vivax* parasites
373 from blood samples

374 *P. vivax* infected blood samples were collected from malaria patients in Tierralta—
375 Córdoba, Colombia, into 5-mL sodium citrate tubes. After transportation to Bogotá,
376 RBCs were enriched by centrifugation, mixed with an equal volume of Glycerolyte 57,
377 cryopreserved, shipped to the U.S. lab, thawed using the NaCl method [61], and
378 resuspended in 3 mL of Iscove's Modified Dulbecco's Medium (IMDM). These RBCs
379 were then enriched from 0.2% to 4.0% parasitemia by concentrating *P. vivax*-infected
380 reticulocytes through a KCl-Percoll gradient [62]. Enrichment was evaluated by
381 microscopy with Giemsa staining (Fig 1A).

382 Identification of the *Plasmodium* species

383 Genomic DNA was extracted from infected cells, and nested PCR was performed using
384 this DNA to identify the *Plasmodium* species. Genus- and species-specific primers
385 targeting the parasite's 18S ribosomal small subunit RNA were used as previously
386 described [63] (see S1 Text).

387 *P. vivax* entry into BEL-A and JK-1 cells

388 The enriched *P. vivax* mono-infected RBC sample (~40 µL) was divided into two equal
389 aliquots, one for co-incubation with BEL-A cells and the other with JK-1 cells. Each cell
390 line ($1.5x10^5$ cells) was cultured in 500 µL of medium, for BEL-A in StemSpan serum-
391 free expansion medium (SFEM, StemCell Technologies), containing 25% human serum

392 (Type AB, Sigma-Aldrich), 50 ng/mL stem cell factor (SCF), 3 U/mL erythropoietin
393 (EPO), 1 μM dexamethasone, 1 μg/mL doxycycline, 1 μg/mL chemically defined lipid
394 concentrate (CDLC), and 100 μM hypoxanthine; and JK-1 in IMDM supplemented with
395 GlutaMAX, with the same components, except for SCF, EPO, dexamethasone, and
396 doxycycline. Both cultures were incubated at 37°C with 5% CO_2 and 5% O_2. Fresh
397 medium and 2×10^5 erythroid cells were added every two days, and cultures were
398 evaluated by immunofluorescence assay (IFA) every 24 hours for 6 days (see S1 Text).

399 Quantitative comparison of membrane proteomes by (DIA) - 400 LC-MS/MS

401 Reticulocytes, erythrocytes, JK-1 and BEL-A cells were collected, cytoplasmic content
402 was removed by osmolytic lysis, and membrane proteins of the remaining ghosts were
403 extracted. From each sample, 23 μg of proteins were processed for proteomics using S-
404 Trap columns (ProtiFi) according to the manufacturer instructions [64,65]. The resulting
405 trypsin/LysC-digested peptides were analyzed by LC-MS/MS in data-independent
406 acquisition (DIA) mode, as detailed in the S1 Text.
407 To enrich the plasma membrane proteins from the data set, proteins were filtered based
408 on at least one of the following annotations from the UniProt subcellular localization
409 database: “Cell membrane”, “Apical cell membrane”, “Basolateral cell membrane”,
410 “Peripheral membrane protein” and “Plasma membrane”, and the Gene Ontology (GO)
411 annotation term: “plasma membrane”. The topology of the membrane proteins abundant
412 in reticulocytes compared to erythrocytes was evaluated using several predictors.
413 Protein sequences were analyzed with Protter for overall visualization of proteoforms

414 [66], TMHMM 2.0 for transmembrane region prediction [67], SignalP 6.0 for signal
415 peptide identification [68], and PredGPI for GPI anchor site prediction [69].

416 PvRBP1A$_{158-650}$ proximity labeling for the identification of 417 likely receptor candidates

418 Cloning, expression, purification, and activity of TurboID fusion 419 proteins

420 The DNA sequence encoding PvRBP1a$_{158-650}$ (GenBank AAS85749.1) was derived
421 from the *P. vivax* Salvador I reference strain (txid126793). This sequence was fused to
422 an acidic linker (L), GDEVDEDEG, to improve solubility, and the TurboID protein (TID)
423 [22], followed by a C-terminal 6xHis tag for purification, resulting in the PvRBP1a$_{158-}$
424 $_{650}$LTID fusion protein. An equivalent gene encoding L with TurboID alone (LTID) was
425 designed as a negative control. Both gene constructs were obtained as customized
426 synthetic genes, optimized for expression in *E. coli,* and cloned into a pET-28a(+)
427 expression vector between its *Nco*I and *Xho*I sites. The constructs were expressed in
428 soluble form in *E. coli* BL21 cells and purified by affinity chromatography, as detailed in
429 the S1 Text. Protein purity and expression were verified by polyacrylamide gel
430 electrophoresis. The biotinylation activity of both recombinant TurboID fusion proteins
431 was confirmed by evaluating their autobiotinylation activity through incubation in the
432 presence or absence of biotinylation reaction buffer Brxn (20 mM Tris-HCl, 500 μM
433 biotin, 2.5 mM ATP, pH 7.5) at 37°C for 15 minutes, quenching on ice and Western blot
434 analysis with streptavidin-IRDye 800CW conjugate (1:1,000) and an Odyssey DLx
435 imaging system (LICORbio).

436 **PvRBP1a$_{158-650}$LTID proximity labeling**

437 To evaluate PvRBP1a$_{158-650}$LTID's interaction with JK-1, BEL-A, reticulocytes, and
438 erythrocytes, proximity labeling assays were performed in duplicate, and repeated up to
439 three times. Cells were washed twice with PBS supplemented with 2% human serum
440 (HS 2%) and incubated with either PvRBP1a$_{158-650}$LTID or LTID (negative control) for 3
441 hours at room temperature with constant mild agitation at 10 rpm. Following incubation,
442 cells were washed three times with HS 2% to remove unbound proteins, then incubated
443 with Brxn for 15 minutes at 37°C. The reaction was stopped by cooling on ice for 5
444 minutes, and the samples were washed with cold HS 2% before labeling with Alexa
445 Fluor 488-conjugated streptavidin (10 µg/mL, Invitrogen) for 1 hour at room
446 temperature. Biotinylation was quantified by cytometry, acquiring 100,000 events per
447 sample on a FACSAria Fusion (BD). Data were analyzed with FlowJo v10.8.1 [70],
448 calculating the percentage of biotinylated cells relative to total cells. LTID-treated and
449 unlabeled cells served as negative controls.

450 **The biochemical nature of PvRBP1a$_{158-650}$ receptors**

451 JK-1 and BEL-A cells were treated with trypsin (1 mg/mL, Sigma-Aldrich), chymotrypsin
452 (1 mg/mL, Sigma-Aldrich), or neuraminidase (50 mU, Roche) for 1 hour. After enzymatic
453 treatment, proteolytic enzymes were inactivated with soy trypsin inhibitor (0.5 mg/mL,
454 Sigma-Gibco) [71]. Proximity labeling assays were then performed as described above,
455 using PvRBP1a$_{158-650}$LTID or LTID (3 µM).

456 **Affinity enrichment and LC-MS identification of PvRBP1a$_{158-650}$**
457 **proximity-labeled receptor candidates**

458 JK-1 cells were incubated with either PvRBP1a$_{158-650}$LTID or LTID (negative control),
459 each at 3 μM for 3 hours. After incubation, cells were washed three times with HS 2%,
460 then incubated with 100 μL of Brxn for 15 minutes at 37°C. The reaction was stopped as
461 described above, and cells were resuspended in 500 μL of IP-MS lysis buffer (MS-
462 compatible Magnetic IP kit, streptavidin, Pierce, Thermo Scientific), incubated on ice for
463 30 minutes with intermittent vortexing every 5 minutes. After centrifugation, the lysate's
464 supernatant was collected and combined with Streptavidin magnetic beads (50 μL,
465 Thermo Scientific), incubated for 1 hour at 21°C, and then overnight at 4°C, to enrich
466 biotinylated membrane proteins. The beads were washed, and biotinylated proteins
467 were eluted sequentially with 100 μL of 50 mM biotin, 100 μL of elution buffer, and 100
468 μL of 5% SDS at 95°C.
469 The eluted proteins were reduced, alkylated, and processed for proteomics using S-
470 Trap spin columns (ProtiFi) according to the manufacturer's instructions [64,65]. The
471 resulting trypsin/LysC digested peptides were analyzed by LC-MS in data-dependent
472 acquisition mode. Data analysis was performed using FragPipe v22.0 [72]. Candidate
473 receptor proteins for PvRBP1a$_{158-650}$ were selected based on the presence of
474 extracellular regions that are favorable for ligand interaction, evaluated using UniProt
475 GO annotations and the TMHMM 2.0 predictor [67]. Receptor candidates in the
476 PvRBP1a$_{158-650}$LTID sample that were detected in both duplicates and of significantly
477 higher abundance (≥ 2 fold) compared to the negative control (LTID) were also
478 considered. Subsequently, a parallel reaction monitoring (PRM) method was applied to
479 validate and quantify the peptides of interest (as detailed in the S1 Text).

480 **Binding affinities of *Pv*RBP1a$_{158-650}$ to select receptor**
481 **candidates by ELISA**

482 The recombinant extracellular protein domains of receptor candidates TfR1 (Cys^{89}-
483 Phe^{760}, SinoBiological), BSG (Met^{1}-His^{205}, SinoBiological), and full-length PHB2
484 (Origene) were used to evaluate the interaction between the PvRBP1a$_{158-650}$ and its
485 binding membrane proteins (S1 Fig). Maxisorp plates were coated in triplicates with 5
486 µg/mL of each protein for 2 hours at room temperature and blocked with SuperBlock
487 Buffer (Thermo Scientific). Serial dilutions of PvRBP1a$_{158-650}$LTID and LTID were
488 prepared in blocking solution, ranging from 48,000 pM to 187.5 pM (1:2 dilution) and
489 4,000 pM to 1.28 pM (1:5 dilution), and incubated for 16 hours at 4°C. Bound
490 PvRBP1a$_{158-650}$LTID and LTID were detected with a TurboID-specific polyclonal rabbit
491 antibody (anti-BirA mutated/TurboID, Agrisera, 1:10,000). After five washes with PBST,
492 100 µL of 3,3',5,5',-Tetramethylbenzidine (TMB) substrate was added, and the reaction
493 was stopped with 50 µL of 1 M phosphoric acid. Absorbance was measured at 450 nm.
494 Dissociation constants (Kd) were determined using GraphPad Prism v10.3.1 with non-
495 linear regression and a one-site binding saturation model.

496 **Acknowledgments**

497 The authors are grateful to NHS Blood and Transplant, especially Professor Jan Frayne,
498 for providing the BEL-A cell line. *"BEL-A cell lines were created by Professor Jan Frayne,*
499 *Professor David Anstee and Dr Kongtana Trakarnsanga with funding from the Wellcome*
500 *Trust (grant numbers 087430/Z/08 and 102610), NHS Blood and Transplant and*
501 *Department of Health (England)"*. Furthermore, they wish to extend their gratitude to the

502 “Grupo de Investigaciones Microbiológicas y Biomédicas de Córdoba – GIMBIC” from the
503 Universidad de Córdoba, Colombia, for providing the *P. vivax* samples. This study was
504 funded in parts by the Memorial Hermann Foundation in support of MK and JMF. The
505 authors dedicate this study to *Professor Manuel Elkin Patarroyo (1946-2025), in loving*
506 *memory.*

507

508 # References

509 1. World Health Organization. World malaria report 2024: addressing inequity in the
510 global malaria response. 2024.

511 2. Malleret B, El Sahili A, Tay MZ, Carissimo G, Ong ASM, Novera W, et al.
512 *Plasmodium vivax* binds host CD98hc (SLC3A2) to enter immature red blood cells.
513 Nat Microbiol. 2021;6: 991–999. doi:10.1038/s41564-021-00939-3

514 3. Gruszczyk J, Kanjee U, Chan L-J, Menant S, Malleret B, Lim NTY, et al. Transferrin
515 receptor 1 is a reticulocyte-specific receptor for *Plasmodium vivax*. Science.
516 2018;359: 48–55. doi:10.1126/science.aan1078

517 4. Molina-Franky J, Patarroyo ME, Kalkum M, Patarroyo MA. The Cellular and
518 Molecular Interaction Between Erythrocytes and *Plasmodium falciparum*
519 Merozoites. Front Cell Infect Microbiol. 2022;12: 816574.
520 doi:10.3389/fcimb.2022.816574

521 5. Malleret B, Li A, Zhang R, Tan KSW, Suwanarusk R, Claser C, et al. Plasmodium
522 vivax: restricted tropism and rapid remodeling of CD71-positive reticulocytes.
523 Blood. 2015;125: 1314–1324. doi:10.1182/blood-2014-08-596015

524 6. Trager W, Jensen JB. Human Malaria Parasites in Continuous Culture. Science.
525 1976;193: 673–675. doi:10.1126/science.781840

526 7. Horuk R, Chitnis CE, Darbonne WC, Colby TJ, Rybicki A, Hadley TJ, et al. A
527 Receptor for the Malarial Parasite *Plasmodium vivax*: the Erythrocyte Chemokine
528 Receptor. Science. 1993;261: 1182–1184. doi:10.1126/science.7689250

529 8. Ryan JR, Stoute JA, Amon J, Dunton RF, Mtalib R, Koros J, et al. Evidence for
530 transmission of *Plasmodium vivax* among a duffy antigen negative population in
531 Western Kenya. Am J Trop Med Hyg. 2006;75: 575–581.

532 9. Reyes C, Picón Jaimes YA, Kalkum M, Patarroyo MA. The Black Box of Cellular and
533 Molecular Events of *Plasmodium vivax* Merozoite Invasion into Reticulocytes.
534 IJMS. 2022;23: 14528. doi:10.3390/ijms232314528

535 10. Picón-Jaimes YA, Lozada-Martinez ID, Orozco-Chinome JE, Molina-Franky J,
536 Acevedo-Lopez D, Acevedo-Lopez N, et al. Relationship between Duffy
537 Genotype/Phenotype and Prevalence of *Plasmodium vivax* Infection: A Systematic
538 Review. TropicalMed. 2023;8: 463. doi:10.3390/tropicalmed8100463

539 11. Galinski MR, Medina CC, Ingravallo P, Barnwell JW. A reticulocyte-binding protein
540 complex of *Plasmodium vivax* merozoites. Cell. 1992;69: 1213–1226.
541 doi:10.1016/0092-8674(92)90642-P

542 12. Urquiza M, Patarroyo M, Marí V, Ocampo M, Suarez J, Lopez R, et al. Identification
543 and polymorphism of *Plasmodium vivax* RBP-1 peptides which bind specifically to
544 reticulocytes. Peptides. 2002;23: 2265–2277. doi:10.1016/S0196-9781(02)00267-X

545 13. Ntumngia FB, Thomson-Luque R, Galusic S, Frato G, Frischmann S, Peabody DS,
546 et al. Identification and Immunological Characterization of the Ligand Domain of
547 *Plasmodium vivax* Reticulocyte Binding Protein 1a. The Journal of Infectious
548 Diseases. 2018;218: 1110–1118. doi:10.1093/infdis/jiy273

549 14. Okuno Y, Suzuki A, Ichiba S, Takahashi T, Nakamura K, Hitomi K, et al.
550 Establishment of an Erythroid Cell Line (JK-1) that Spontaneously Diferentiates to
551 Red Cells. 66: 8.

552 15. Trakarnsanga K, Griffiths RE, Wilson MC, Blair A, Satchwell TJ, Meinders M, et al.
553 An immortalized adult human erythroid line facilitates sustainable and scalable
554 generation of functional red cells. Nat Commun. 2017;8: 14750.
555 doi:10.1038/ncomms14750

556 16. Cao P, Kho S, Grigg MJ, Barber BE, Piera KA, William T, et al. Characterisation of
557 *Plasmodium vivax* lactate dehydrogenase dynamics in *Plasmodium vivax*
558 infections. Commun Biol. 2024;7: 355. doi:10.1038/s42003-024-05956-6

559 17. Pandey AV, Tekwani BL. Formation of haemozoin/β-haematin under physiological
560 conditions is not spontaneous. FEBS Letters. 1996;393: 189–192.
561 doi:10.1016/0014-5793(96)00881-2

562 18. Coronado LM, Nadovich CT, Spadafora C. Malarial hemozoin: From target to tool.
563 Biochimica et Biophysica Acta (BBA) - General Subjects. 2014;1840: 2032–2041.
564 doi:10.1016/j.bbagen.2014.02.009

565 19. Carlton JM, Adams JH, Silva JC, Bidwell SL, Lorenzi H, Caler E, et al. Comparative
566 genomics of the neglected human malaria parasite *Plasmodium vivax*. Nature.
567 2008;455: 757–763. doi:10.1038/nature07327

568 20. Malleret B, Li A, Zhang R, Tan KSW, Suwanarusk R, Claser C, et al. *Plasmodium*
569 *vivax*: restricted tropism and rapid remodeling of CD71-positive reticulocytes.
570 Blood. 2015;125: 1314–1324. doi:10.1182/blood-2014-08-596015

571 21. Lex A, Gehlenborg N, Strobelt H, Vuillemot R, Pfister H. UpSet: Visualization of
572 Intersecting Sets. IEEE Trans Visual Comput Graphics. 2014;20: 1983–1992.
573 doi:10.1109/TVCG.2014.2346248

574 22. Branon TC, Bosch JA, Sanchez AD, Udeshi ND, Svinkina T, Carr SA, et al.
575 Efficient proximity labeling in living cells and organisms with TurboID. Nat
576 Biotechnol. 2018;36: 880–887. doi:10.1038/nbt.4201

577 23. Cho KF, Branon TC, Udeshi ND, Myers SA, Carr SA, Ting AY. Proximity labeling in
578 mammalian cells with TurboID and split-TurboID. Nat Protoc. 2020;15: 3971–3999.
579 doi:10.1038/s41596-020-0399-0

580 24. Kanjee U, Grüring C, Chaand M, Lin K-M, Egan E, Manzo J, et al. CRISPR/Cas9
581 knockouts reveal genetic interaction between strain-transcendent erythrocyte
582 determinants of *Plasmodium falciparum* invasion. Proc Natl Acad Sci U S A.
583 2017;114: E9356–E9365. doi:10.1073/pnas.1711310114

584 25. Gruszczyk J, Kanjee U, Chan L-J, Menant S, Malleret B, Lim NTY, et al. Transferrin
585 receptor 1 is a reticulocyte-specific receptor for *Plasmodium vivax*. Science.
586 2018;359: 48–55. doi:10.1126/science.aan1078

587 26. Satchwell TJ, Wright KE, Haydn-Smith KL, Sánchez-Román Terán F, Moura PL,
588 Hawksworth J, et al. Genetic manipulation of cell line derived reticulocytes enables
589 dissection of host malaria invasion requirements. Nat Commun. 2019;10: 3806.
590 doi:10.1038/s41467-019-11790-w

591 27. Smith JosephD, Kyes S, Craig AlisterG, Fagan T, Hudson-Taylor D, Miller LouisH,
592 et al. Analysis of adhesive domains from the A4VAR Plasmodium falciparum
593 erythrocyte membrane protein-1 identifies a CD36 binding domain. Molecular and
594 Biochemical Parasitology. 1998;97: 133–148. doi:10.1016/S0166-6851(98)00145-5

595 28. Albritton LM, Kim JW, Tseng L, Cunningham JM. Envelope-binding domain in the
596 cationic amino acid transporter determines the host range of ecotropic murine
597 retroviruses. J Virol. 1993;67: 2091–2096. doi:10.1128/jvi.67.4.2091-2096.1993

598 29. Yoshimoto T, Yoshimoto E, Meruelo D. Identification of amino acid residues critical
599 for infection with ecotropic murine leukemia retrovirus. J Virol. 1993;67: 1310–
600 1314. doi:10.1128/jvi.67.3.1310-1314.1993

601 30. Olaya-Galán NN, Salas-Cárdenas SP, Rodriguez-Sarmiento JL, Ibáñez-Pinilla M,
602 Monroy R, Corredor-Figueroa AP, et al. Risk factor for breast cancer development
603 under exposure to bovine leukemia virus in Colombian women: A case-control
604 study. Jaworski JP, editor. PLoS ONE. 2021;16: e0257492.
605 doi:10.1371/journal.pone.0257492

606 31. Tailor CS, Nouri A, Zhao Y, Takeuchi Y, Kabat D. A sodium-dependent neutral-
607 amino-acid transporter mediates infections of feline and baboon endogenous
608 retroviruses and simian type D retroviruses. J Virol. 1999;73: 4470–4474.
609 doi:10.1128/JVI.73.5.4470-4474.1999

610 32. Feire AL, Roy RM, Manley K, Compton T. The Glycoprotein B Disintegrin-Like
611 Domain Binds Beta 1 Integrin To Mediate Cytomegalovirus Entry. J Virol. 2010;84:
612 10026–10037. doi:10.1128/JVI.00710-10

613 33. Xiao J, Palefsky JM, Herrera R, Berline J, Tugizov SM. The Epstein–Barr virus
614 BMRF-2 protein facilitates virus attachment to oral epithelial cells. Virology.
615 2008;370: 430–442. doi:10.1016/j.virol.2007.09.012

616 34. Weigel-Kelley KA, Yoder MC, Srivastava A. α5β1 integrin as a cellular coreceptor
617 for human parvovirus B19: requirement of functional activation of β1 integrin for
618 viral entry. Blood. 2003;102: 3927–3933. doi:10.1182/blood-2003-05-1522

619 35. Graham KL, Halasz P, Tan Y, Hewish MJ, Takada Y, Mackow ER, et al. Integrin-
620 Using Rotaviruses Bind α2β1 Integrin α2 I Domain via VP4 DGE Sequence and
621 Recognize αXβ2 and αVβ3 by Using VP7 during Cell Entry. J Virol. 2003;77: 9969–
622 9978. doi:10.1128/JVI.77.18.9969-9978.2003

623 36. Maginnis MS, Forrest JC, Kopecky-Bromberg SA, Dickeson SK, Santoro SA, Zutter
624 MM, et al. Beta1 integrin mediates internalization of mammalian reovirus. J Virol.
625 2006;80: 2760–2770. doi:10.1128/JVI.80.6.2760-2770.2006

626 37. Nägele V, Heesemann J, Schielke S, Jiménez-Soto LF, Kurzai O, Ackermann N.
627 Neisseria meningitidis adhesin NadA targets beta1 integrins: functional similarity to
628 Yersinia invasin. J Biol Chem. 2011;286: 20536–20546.
629 doi:10.1074/jbc.M110.188326

630 38. Wintachai P, Wikan N, Kuadkitkan A, Jaimipuk T, Ubol S, Pulmanausahakul R, et
631 al. Identification of prohibitin as a Chikungunya virus receptor protein. J Med Virol.
632 2012;84: 1757–1770. doi:10.1002/jmv.23403

633 39. Su W, Huang S, Zhu H, Zhang B, Wu X. Interaction between PHB2 and
634 Enterovirus A71 VP1 Induces Autophagy and Affects EV-A71 Infection. Viruses.
635 2020;12: 414. doi:10.3390/v12040414

636 40. Lee Y, Wiriyasermkul P, Jin C, Quan L, Ohgaki R, Okuda S, et al. Cryo-EM
637 structure of the human L-type amino acid transporter 1 in complex with
638 glycoprotein CD98hc. Nat Struct Mol Biol. 2019;26: 510–517. doi:10.1038/s41594-
639 019-0237-7

640 41. Yan R, Zhao X, Lei J, Zhou Q. Structure of the human LAT1–4F2hc heteromeric
641 amino acid transporter complex. Nature. 2019;568: 127–130. doi:10.1038/s41586-
642 019-1011-z

643 42. Nguyen NNT, Lim Y-S, Nguyen LP, Tran SC, Luong TTD, Nguyen TTT, et al.
644 Hepatitis C Virus Modulates Solute carrier family 3 member 2 for Viral Propagation.
645 Sci Rep. 2018;8: 15486. doi:10.1038/s41598-018-33861-6

646 43. Han J-H, Lee S-K, Wang B, Muh F, Nyunt MH, Na S, et al. Identification of a
647 reticulocyte-specific binding domain of *Plasmodium vivax* reticulocyte-binding
648 protein 1 that is homologous to the PfRh4 erythrocyte-binding domain. Sci Rep.
649 2016;6: 26993. doi:10.1038/srep26993

650 44. Gupta ED, Anand G, Singh H, Chaddha K, Bharti PK, Singh N, et al. Naturally
651 Acquired Human Antibodies Against Reticulocyte-Binding Domains of *Plasmodium*
652 *vivax* Proteins, PvRBP2c and PvRBP1a, Exhibit Binding-Inhibitory Activity. J Infect
653 Dis. 2017;215: 1558–1568. doi:10.1093/infdis/jix170

654 45. Radoshitzky SR, Kuhn JH, Spiropoulou CF, Albariño CG, Nguyen DP, Salazar-
655 Bravo J, et al. Receptor determinants of zoonotic transmission of New World
656 hemorrhagic fever arenaviruses. Proc Natl Acad Sci USA. 2008;105: 2664–2669.
657 doi:10.1073/pnas.0709254105

658 46. Radoshitzky SR, Abraham J, Spiropoulou CF, Kuhn JH, Nguyen D, Li W, et al.
659 Transferrin receptor 1 is a cellular receptor for New World haemorrhagic fever
660 arenaviruses. Nature. 2007;446: 92–96. doi:10.1038/nature05539

661 47. Crosnier C, Bustamante LY, Bartholdson SJ, Bei AK, Theron M, Uchikawa M, et al.
662 Basigin is a receptor essential for erythrocyte invasion by *Plasmodium falciparum*.
663 Nature. 2011;480: 534–537. doi:10.1038/nature10606

664 48. Chen L, Xu Y, Healer J, Thompson JK, Smith BJ, Lawrence MC, et al. Crystal
665 structure of PfRh5, an essential *Plasmodium falciparum* ligand for invasion of
666 human erythrocytes. eLife. 2014;3: e04187. doi:10.7554/eLife.04187

667 49. Rayner JC, Galinski MR, Ingravallo P, Barnwell JW. Two Plasmodium falciparum
668 genes express merozoite proteins that are related to Plasmodium vivax and
669 Plasmodium yoelii adhesive proteins involved in host cell selection and invasion.
670 Proceedings of the National Academy of Sciences. 2000;97: 9648–9653.
671 doi:10.1073/pnas.160469097

672 50. Triglia T, Thompson J, Caruana SR, Delorenzi M, Speed T, Cowman AF.
673 Identification of Proteins from Plasmodium falciparum That Are Homologous to
674 Reticulocyte Binding Proteins in Plasmodium vivax. Petri WA, editor. Infect Immun.
675 2001;69: 1084–1092. doi:10.1128/IAI.69.2.1084-1092.2001

676 51. Rathore S, Dass S, Kandari D, Kaur I, Gupta M, Sharma YD. Basigin Interacts with
677 *Plasmodium vivax*Tryptophan-rich Antigen PvTRAg38 as a Second Erythrocyte
678 Receptor to Promote Parasite Growth. J Biol Chem. 2017;292: 462–476.
679 doi:10.1074/jbc.M116.744367

680 52. Emerson V, Holtkotte D, Pfeiffer T, Wang I-H, Schnölzer M, Kempf T, et al.
681 Identification of the Cellular Prohibitin 1/Prohibitin 2 Heterodimer as an Interaction
682 Partner of the C-Terminal Cytoplasmic Domain of the HIV-1 Glycoprotein. J Virol.
683 2010;84: 1355–1365. doi:10.1128/JVI.01641-09

684 53. Cornillez-Ty CT, Liao L, Yates JR, Kuhn P, Buchmeier MJ. Severe acute
685 respiratory syndrome coronavirus nonstructural protein 2 interacts with a host
686 protein complex involved in mitochondrial biogenesis and intracellular signaling. J
687 Virol. 2009;83: 10314–10318. doi:10.1128/JVI.00842-09

688 54. Kuadkitkan A, Wikan N, Fongsaran C, Smith DR. Identification and characterization
689 of prohibitin as a receptor protein mediating DENV-2 entry into insect cells.
690 Virology. 2010;406: 149–161. doi:10.1016/j.virol.2010.07.015

691 55. Alam MS, Rathore S, Tyagi RK, Sharma YD. Host-parasite interaction: multiple
692 sites in the *Plasmodium vivax* tryptophan-rich antigen PvTRAg38 interact with the
693 erythrocyte receptor band 3. Griesinger C, editor. FEBS Lett. 2016;590: 232–241.
694 doi:10.1002/1873-3468.12053

695 56. Yipp BG, Anand S, Schollaardt T, Patel KD, Looareesuwan S, Ho M. Synergism of
696 multiple adhesion molecules in mediating cytoadherence of *Plasmodium*
697 *falciparum*–infected erythrocytes to microvascular endothelial cells under flow.
698 Blood. 2000;96: 2292–2298. doi:10.1182/blood.V96.6.2292

699 57. Vogt AM, Barragan A, Chen Q, Kironde F, Spillmann D, Wahlgren M. Heparan
700 sulfate on endothelial cells mediates the binding of *Plasmodium falciparum*–
701 infected erythrocytes via the DBL1α domain of PfEMP1. Blood. 2003;101: 2405–
702 2411. doi:10.1182/blood-2002-07-2016

703 58. Vigan-Womas I, Guillotte M, Juillerat A, Hessel A, Raynal B, England P, et al.
704 Structural Basis for the ABO Blood-Group Dependence of *Plasmodium falciparum*
705 Rosetting. Rowe JA, editor. PLoS Pathog. 2012;8: e1002781.
706 doi:10.1371/journal.ppat.1002781

707 59. Kessler A, Dankwa S, Bernabeu M, Harawa V, Danziger SA, Duffy F, et al. Linking
708 EPCR-Binding PfEMP1 to Brain Swelling in Pediatric Cerebral Malaria. Cell Host &
709 Microbe. 2017;22: 601-614.e5. doi:10.1016/j.chom.2017.09.009

710 60. Esser C, Bachmann A, Kuhn D, Schuldt K, Förster B, Thiel M, et al. Evidence of
711 promiscuous endothelial binding by *Plasmodium falciparum*-infected erythrocytes.
712 Cell Microbiol. 2014;16: 701–708. doi:10.1111/cmi.12270

713 61. Blomqvist, K. Thawing of glycerolyte-frozen parasites with NaCl. Methods in
714 Malaria Research. MR4/ATCC, Manassas. Methods in Malaria Research. Methods
715 in Malaria Research. MR4/ATCC, Manassas. 2008. p. 15.

716 62. Rangel GW, Clark MA, Kanjee U, Lim C, Shaw-Saliba K, Menezes MJ, et al.
717 Enhanced ex vivo *Plasmodium vivax* Intraerythrocytic Enrichment and Maturation

for Rapid and Sensitive Parasite Growth Assays. Antimicrob Agents Chemother. 2018;62: e02519-17. doi:10.1128/AAC.02519-17

63. Snounou G, Viriyakosol S, Xin Ping Zhu, Jarra W, Pinheiro L, Do Rosario VE, et al. High sensitivity of detection of human malaria parasites by the use of nested polymerase chain reaction. Molecular and Biochemical Parasitology. 1993;61: 315–320. doi:10.1016/0166-6851(93)90077-B

64. HaileMariam M, Eguez RV, Singh H, Bekele S, Ameni G, Pieper R, et al. S-Trap, an Ultrafast Sample-Preparation Approach for Shotgun Proteomics. J Proteome Res. 2018;17: 2917–2924. doi:10.1021/acs.jproteome.8b00505

65. Matulis D. Selective Precipitation of Proteins. CP Protein Science. 2016;83. doi:10.1002/0471140864.ps0405s83

66. Omasits U, Ahrens CH, Müller S, Wollscheid B. Protter: interactive protein feature visualization and integration with experimental proteomic data. Bioinformatics. 2014;30: 884–886. doi:10.1093/bioinformatics/btt607

67. Hallgren J, Tsirigos KD, Pedersen MD, Almagro Armenteros JJ, Marcatili P, Nielsen H, et al. DeepTMHMM predicts alpha and beta transmembrane proteins using deep neural networks. Bioinformatics; 2022 Apr. doi:10.1101/2022.04.08.487609

68. Teufel F, Almagro Armenteros JJ, Johansen AR, Gíslason MH, Pihl SI, Tsirigos KD, et al. SignalP 6.0 predicts all five types of signal peptides using protein language models. Nat Biotechnol. 2022;40: 1023–1025. doi:10.1038/s41587-021-01156-3

69. Pierleoni A, Martelli PL, Casadio R. PredGPI: a GPI-anchor predictor. BMC Bioinformatics. 2008;9: 392. doi:10.1186/1471-2105-9-392

70. Ashland, OR: Becton, Dickinson and Company. FlowJo™ Software (for Windows) Version 10.8.1. 2023.

71. Deans A-M, Nery S, Conway DJ, Kai O, Marsh K, Rowe JA. Invasion Pathways and Malaria Severity in Kenyan *Plasmodium falciparum* Clinical Isolates. Infect Immun. 2007;75: 3014–3020. doi:10.1128/IAI.00249-07

72. Yu F, Haynes SE, Nesvizhskii AI. IonQuant Enables Accurate and Sensitive Label-Free Quantification With FDR-Controlled Match-Between-Runs. Molecular & Cellular Proteomics. 2021;20: 100077. doi:10.1016/j.mcpro.2021.100077

Supporting information captions

S1 Text. Supporting methods.

752 **S1 Table. *P. vivax* merozoite candidate receptors**

753 **S1 Fig. Purity Analysis of Recombinant Proteins.**

754 Recombinant proteins BSG, TfR1, and PHB2 were separated on a 4–12%
755 polyacrylamide gel and stained with Coomassie blue. The observed bands correspond
756 to the expected molecular weights for each protein: BSG (35 kDa), TfR1 (~77.4 kDa),
757 and PHB2 (~35.7 kDa), confirming their purity. The Kaleidoscope molecular weight
758 marker (Bio-Rad) is included in the left lane as a reference.

759 **S2 Fig. Reticulocyte enrichment.**

760 (A, B) Reticulocyte percentage in the initial whole blood sample. (C, D) Reticulocyte
761 percentage after Percoll density (70%-62%) enrichment. (E) Purity of reticulocytes
762 ($CD71^+$ $CD45^-$) after sorting collection. This high-purity reticulocyte sample was not
763 evaluated with brilliant cresyl blue due to the small total volume of sample obtained (~
764 50 µL). (B, D) Blood smears stained with brilliant cresyl blue to identify reticulocytes (red
765 arrows). Scale bars are 10 µm.

766 **S3 Fig. Differentiation of erythroid cells.**

767 (A-D) BEL-A cells. (E-H) JK-1 cells. (A, E) Proerythroblasts (20-25 µm) were identified
768 by their large nucleus with fine chromatin, prominent nucleoli, and basophilic cytoplasm.
769 These cells progressed to (B, F) Basophilic erythroblasts (16-18 µm), characterized by a
770 slightly smaller nucleus with condensed chromatin and cytoplasm with pronounced
771 basophilia due to increased ribosomes synthesizing Hb. Subsequently, cells
772 differentiated into (C, G) polychromatophilic erythroblasts (12-15 µm), which exhibited a
773 more condensed nucleus with clusters of heterochromatin. The final nucleated stage,
774 (D, H) orthochromatic erythroblast, indicated by the red arrow in D (10-12 µm), was

775 noted for its pyknotic nucleus and a cytoplasm rich in acidophilic Hb. At this stage, the
776 nucleus is expelled to form reticulocytes (8-10 μm), which then mature into erythrocytes
777 (7-8 μm) through the final step of erythroid differentiation.

778 **S4 Fig. Gene Ontology (GO) term analysis of plasma membrane proteins.**
779 Scatterplots showing the GO terms: cellular component, molecular function, and
780 biological process of enriched plasma membrane proteins. The bubble color indicates
781 the count of the GO term, which was obtained from the DAVID functional annotation
782 charts. The size of the bubbles indicates the frequency of the GO term in the Gene
783 Ontology Annotation (GOA) database. The axes of the plot have no intrinsic meaning.
784 REVIGO (version 1.8.1) was used to generate these scatterplots by reducing the
785 dimensionality of a pairwise semantic similarity matrix of GO terms using
786 Multidimensional Scaling (MDS). The resulting projection is not nonlinear. The guiding
787 principle is that semantically similar GO terms should remain close together in the plot.

788 **S5 Fig. Topology of *P. vivax* merozoite receptor candidates.**
789 (A-J) Predicted locations of potential parasite receptors are illustrated for the signal
790 peptide (yellow), extracellular domain (blue), intracellular domain (mauve), and
791 membrane-embedded domain (red).

792 **S6 Fig. Reticulocyte enrichment process.**
793 (A) Initial percentage of reticulocytes in the whole blood sample (0.11%). (B)
794 Percentage of reticulocytes after enrichment using a 70%-62% Percoll density gradient
795 (10.5%). (C) Final percentage of reticulocytes ($CD45^-$ and $CD98^+$) following FACS
796 sorting (87.5%).

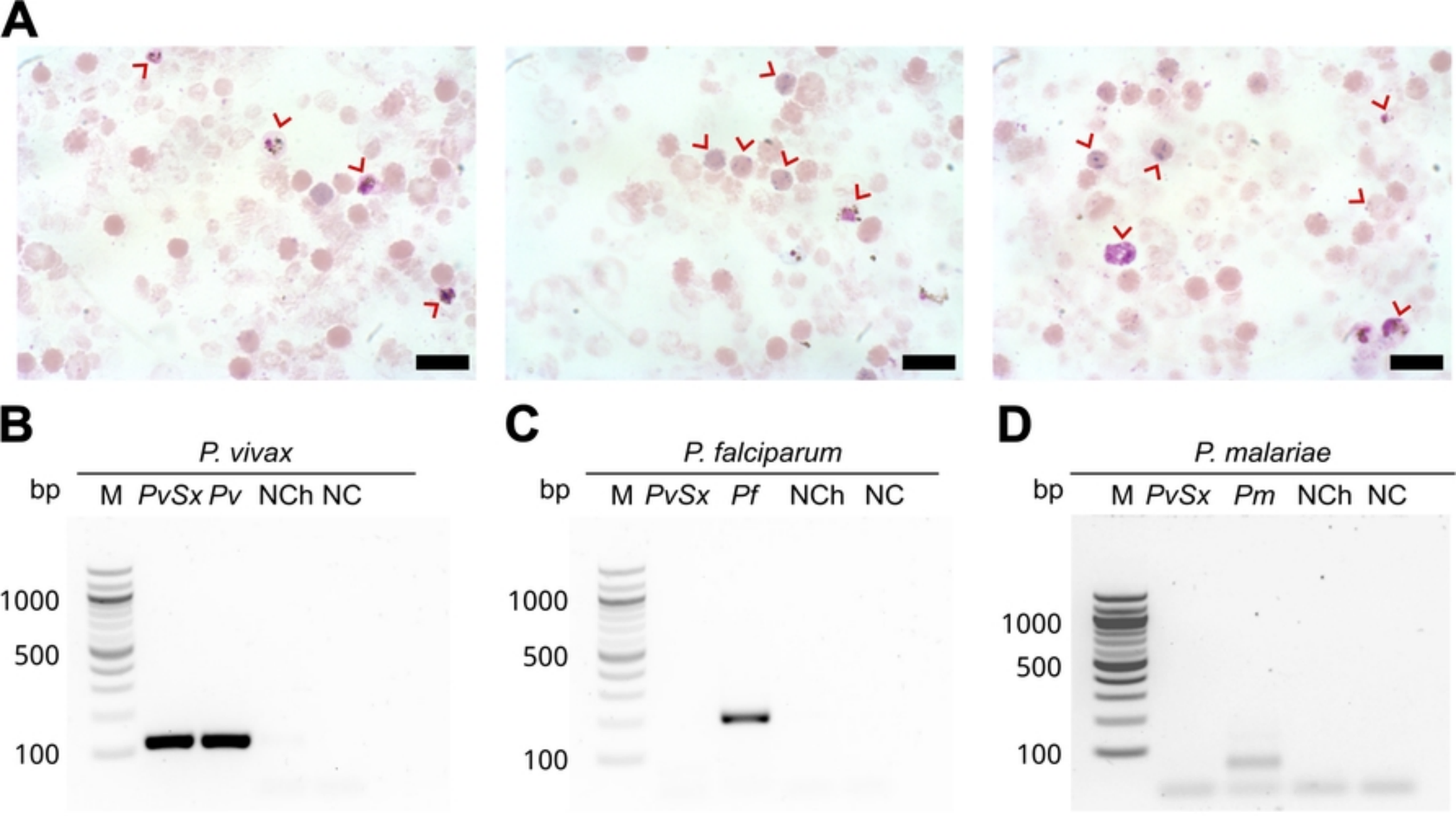

E

```
PvSx            1    TTCTAGCTTAATCCACATAACTGATACTTCGTATCGACTTTGTGCGCATTTTGCTATTAT   60
                     ||||||||||||||||||||||||||||||||||||||||||||||||||||||||||||
XR_003001206.1  669  TTCTAGCTTAATCCACATAACTGATACTTCGTATCGACTTTGTGCGCATTTTGCTATTAT  728

PvSx            61   GTGTTCTTTTAATTAAAATGATTCTTTTTAAGGACTTTCTTTGCTTCGGCTTGGA   115
                     |||||||||||||||||||||||||||||||||||||||||||||||||||||||
XR_003001206.1  729  GTGTTCTTTTAATTAAAATGATTCTTTTTAAGGACTTTCTTTGCTTCGGCTTGGA   783
```

Figure 1

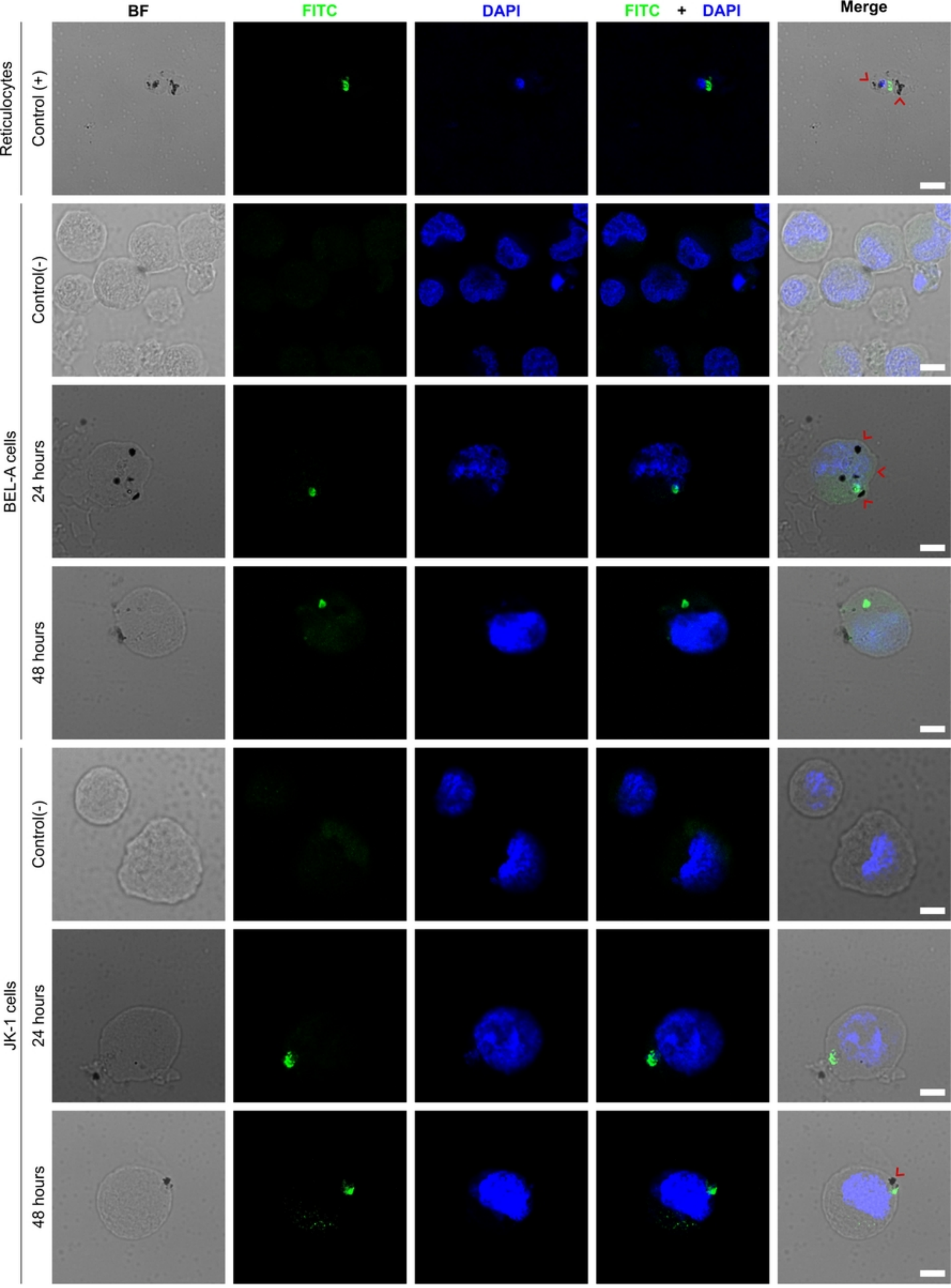
BF
FITC
DAPI
FITC + DAPI
Merge
Reticulocytes
Control (+)
BEL-A cells
Control(-)
24 hours
48 hours
JK-1 cells
Control(-)
24 hours
48 hours

Figure 2

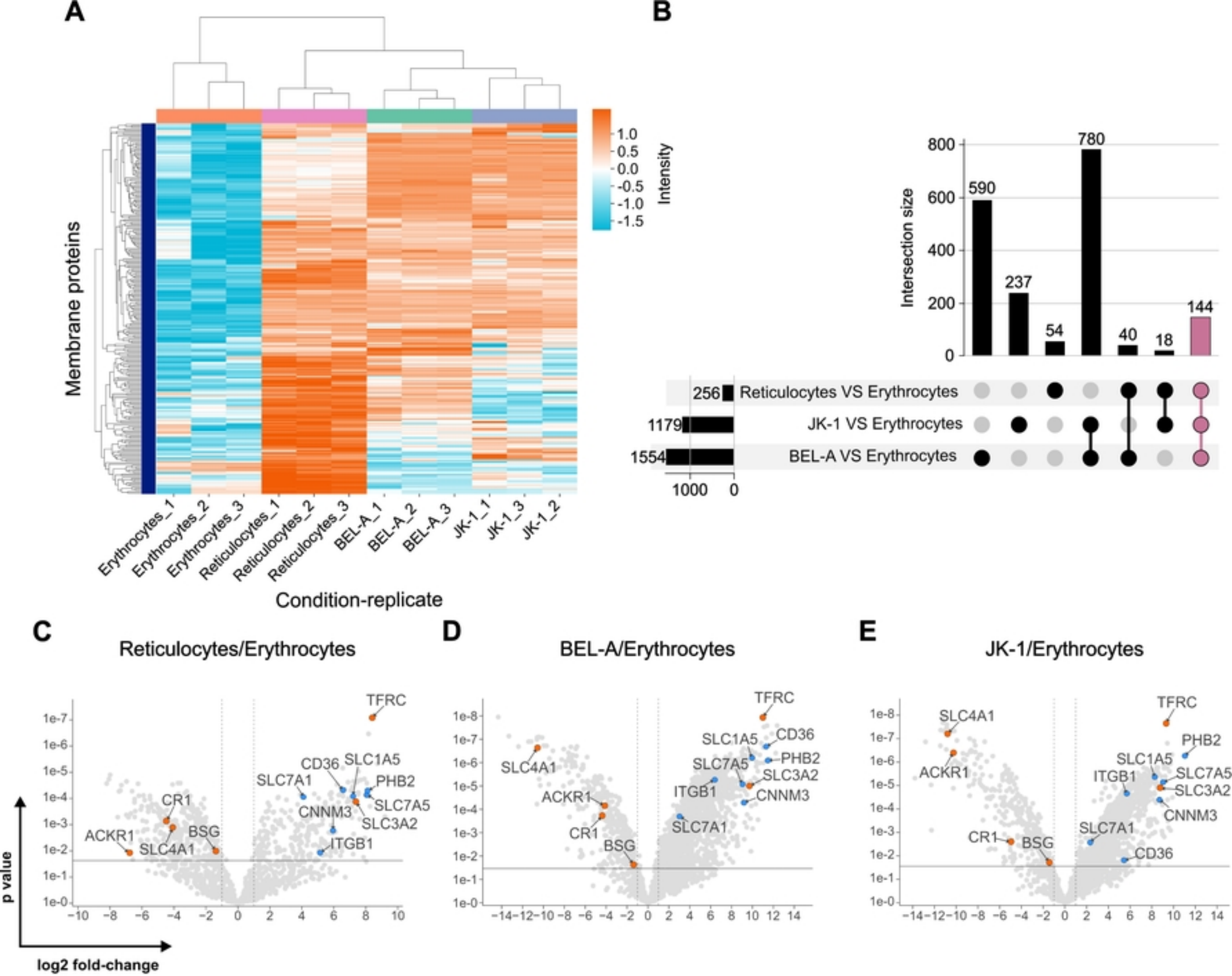
A
Membrane proteins
Intensity
1.0
0.5
0.0
-0.5
-1.0
-1.5
Erythrocytes_1
Erythrocytes_2
Erythrocytes_3
Reticulocytes_1
Reticulocytes_2
Reticulocytes_3
BEL-A_1
BEL-A_2
BEL-A_3
JK-1_1
JK-1_3
JK-1_2
Condition-replicate
B
Intersection size
590
237
54
780
40
18
144
256
1179
1554
Reticulocytes VS Erythrocytes
JK-1 VS Erythrocytes
BEL-A VS Erythrocytes
C
Reticulocytes/Erythrocytes
D
BEL-A/Erythrocytes
E
JK-1/Erythrocytes
TFRC
CD36
SLC1A5
SLC7A1
PHB2
CR1
CNNM3
SLC7A5
SLC3A2
ACKR1
BSG
SLC4A1
ITGB1
p value
log2 fold-change

Figure 3

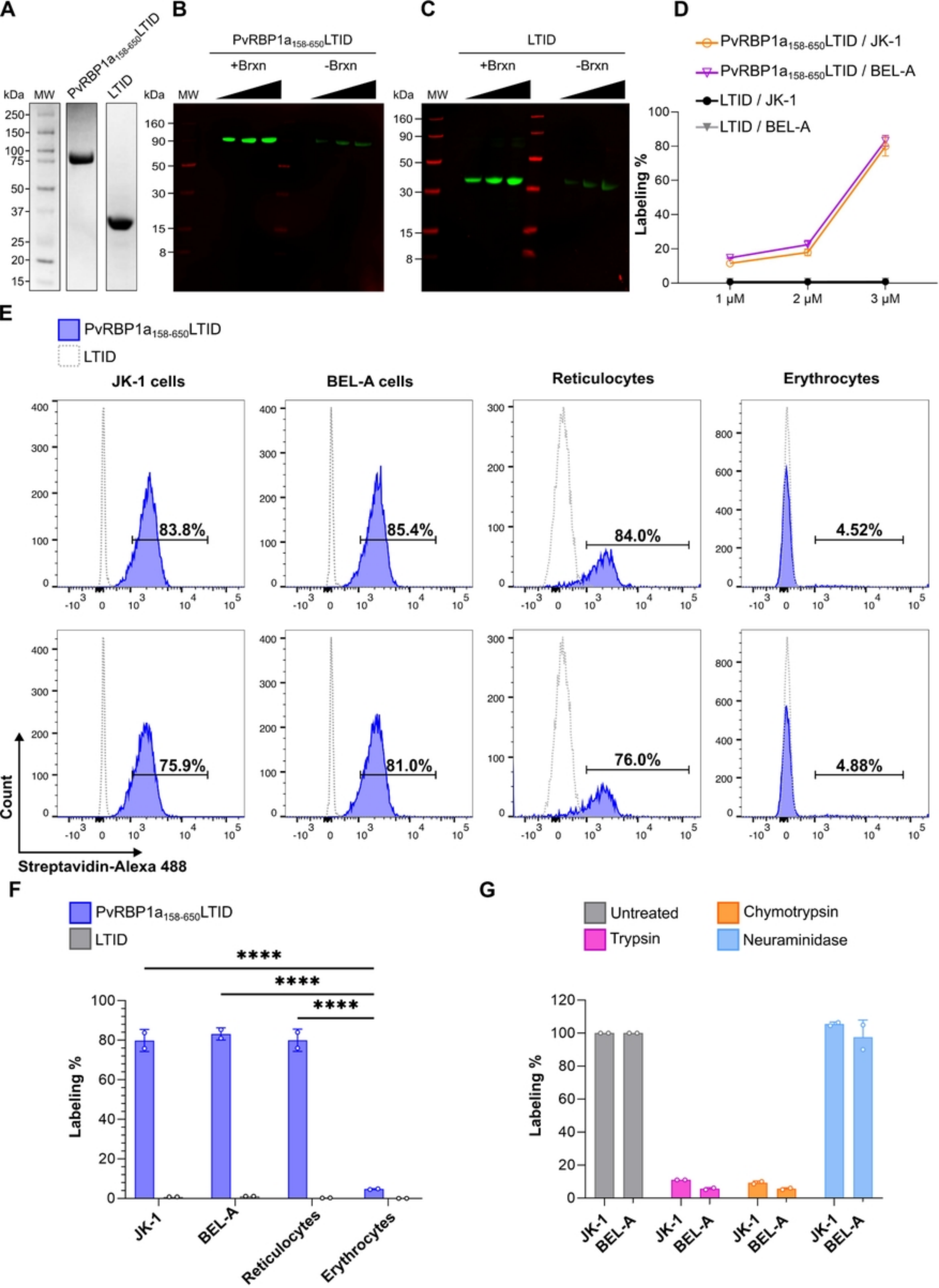
A
PvRBP1a158-650LTID
LTID
kDa
MW
250
150
100
75
50
37
25
20
15
B
PvRBP1a158-650LTID
+Brxn
-Brxn
160
90
50
30
15
8
C
LTID
D
PvRBP1a158-650LTID / JK-1
PvRBP1a158-650LTID / BEL-A
LTID / JK-1
LTID / BEL-A
Labeling %
1 μM
2 μM
3 μM
E
PvRBP1a158-650LTID
LTID
JK-1 cells
BEL-A cells
Reticulocytes
Erythrocytes
83.8%
85.4%
84.0%
4.52%
75.9%
81.0%
76.0%
4.88%
Count
Streptavidin-Alexa 488
F
PvRBP1a158-650LTID
LTID
****
Labeling %
JK-1
BEL-A
Reticulocytes
Erythrocytes
G
Untreated
Chymotrypsin
Trypsin
Neuraminidase
Labeling %
JK-1
BEL-A

Figure 4

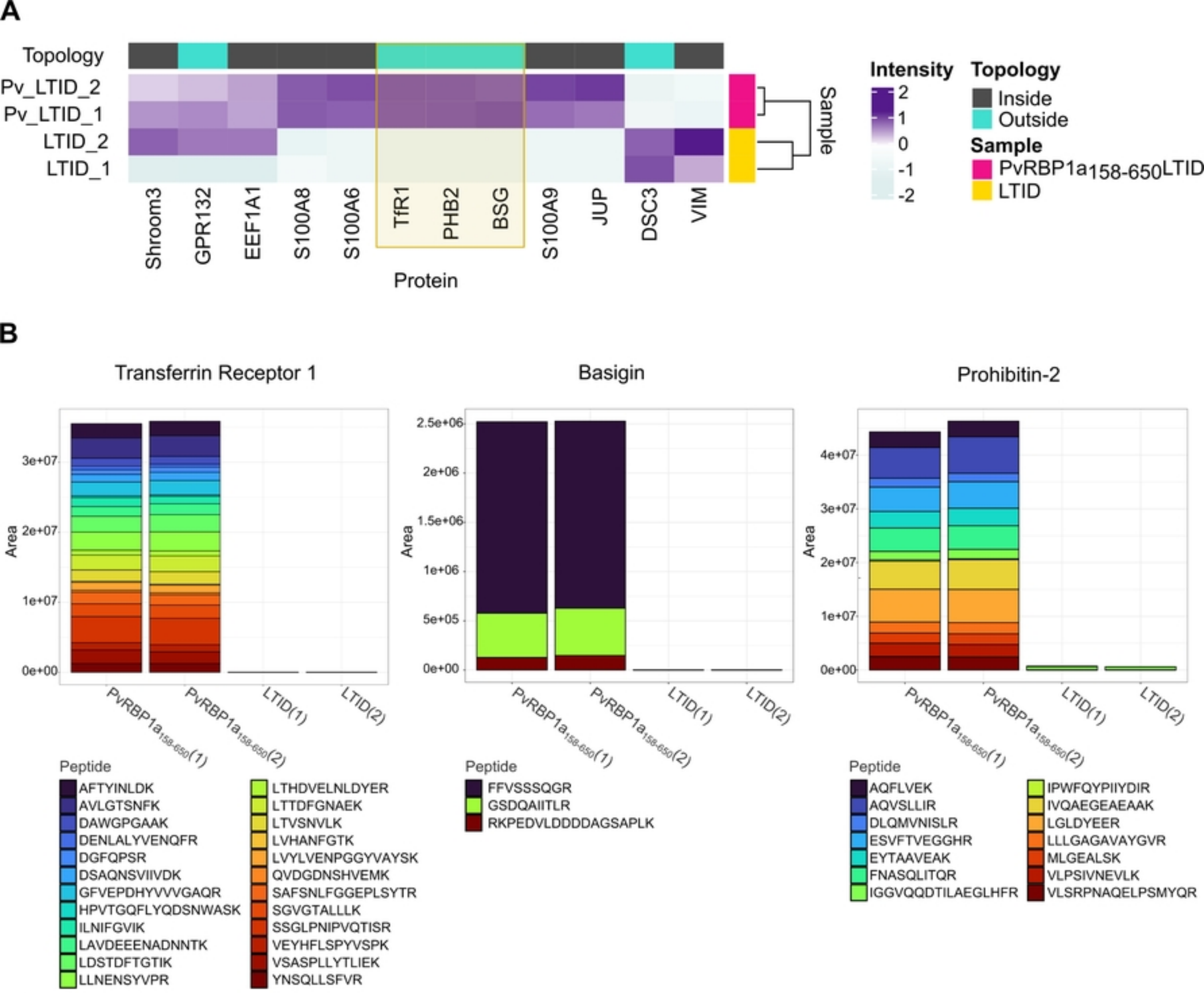
A
Topology
Pv_LTID_2
Pv_LTID_1
LTID_2
LTID_1
Shroom3
GPR132
EEF1A1
S100A8
S100A6
TfR1
PHB2
BSG
S100A9
JUP
DSC3
VIM
Protein
Sample
Intensity
2
1
0
-1
-2
Topology
Inside
Outside
Sample
PvRBP1a158-650LTID
LTID
B
Transferrin Receptor 1
Basigin
Prohibitin-2
Area
3e+07
2e+07
1e+07
0e+00
2.5e+06
2e+06
1.5e+06
1e+06
5e+05
4e+07
PvRBP1a158-650(1)
PvRBP1a158-650(2)
LTID(1)
LTID(2)
Peptide
AFTYINLDK
AVLGTSNFK
DAWGPGAAK
DENLALYVENQFR
DGFQPSR
DSAQNSVIIVDK
GFVEPDHYVVVGAQR
HPVTGQFLYQDSNWASK
ILNIFGVIK
LAVDEEENADNNTK
LDSTDFTGTIK
LLNENSYVPR
LTHDVELNLDYER
LTTDFGNAEK
LTVSNVLK
LVHANFGTK
LVYLVENPGGYVAYSK
QVDGDNSHVEMK
SAFSNLFGGEPLSYTR
SGVGTALLLK
SSGLPNIPVQTISR
VEYHFLSPYVSPK
VSASPLLYTLIEK
YNSQLLSFVR
FFVSSSQGR
GSDQAIITLR
RKPEDVLDDDDAGSAPLK
AQFLVEK
AQVSLLIR
DLQMVNISLR
ESVFTVEGGHR
EYTAAVEAK
FNASQLITQR
IGGVQQDTILAEGLHFR
IPWFQYPIIYDIR
IVQAEGEAEAAK
LGLDYEER
LLLGAGAVAYGVR
MLGEALSK
VLPSIVNEVLK
VLSRPNAQELPSMYQR

Figure 5

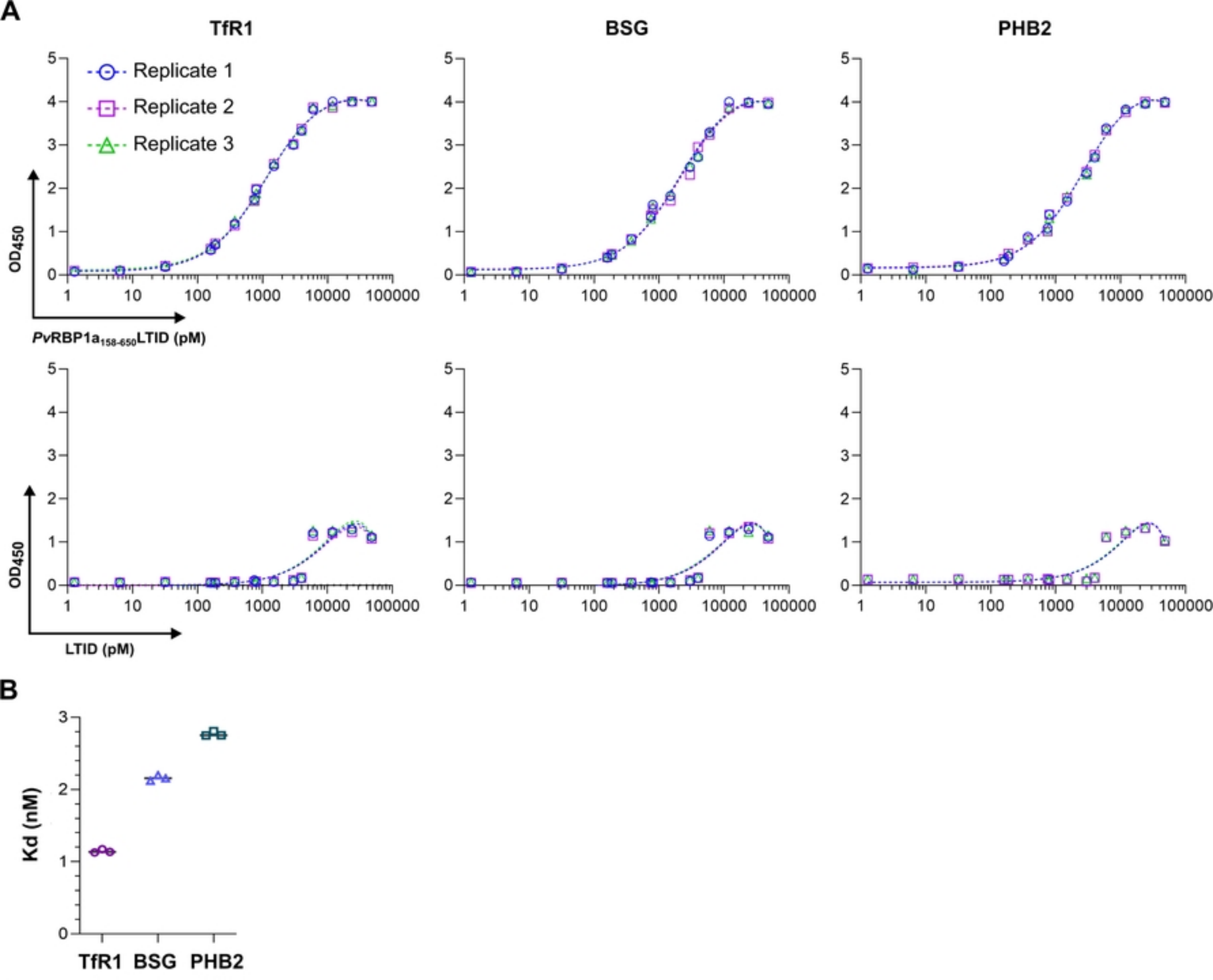
A
TfR1
BSG
PHB2
Replicate 1
Replicate 2
Replicate 3
OD450
PvRBP1a158-650LTID (pM)
LTID (pM)
B
Kd (nM)
TfR1
BSG
PHB2

Figure 6